Oxidation of Cyanide-bridged Dimanganese(I) Complexes: Redox-induced Isomerisation as a Probe of Intermetallic Interaction *

Gabino A. Carriedo,[a] Neil G. Connelly,[b] M. Carmen Crespo,[a] Ian C. Quarmby,[b] Victor Riera[a] and Gillian H. Worth[b]

[a] *Department of Organometallic Chemistry, University of Oviedo, Oviedo 33071, Spain*
[b] *School of Chemistry, University of Bristol, Bristol BS8 1TS, UK*

The reaction of $[Mn(CN)(CO)_2L(L–L)]$ with $[MnBr(CO)_2L'(L'–L')]$ in the presence of $TlPF_6$ gives $[(L–L)L(OC)_2Mn(\mu\text{-}CN)Mn(CO)_2L'(L'–L')][PF_6]$ which may have *trans,trans*; *cis,trans*; *trans,cis* or *cis,cis* geometries depending on the structures of the mononuclear precursors. The *trans,trans* complexes undergo two reversible one-electron oxidations, the first at the N-bonded $Mn(CO)_2L'(L'–L')$ site to give dications which IR carbonyl and ESR spectroscopy and cyclic voltammetry suggest to be localised mixed-valence species. The oxidation of the *cis,trans* and *trans,cis* monocations occurs first at the *trans* site and then at the *cis* site. Where the difference in potential, Δ, between the two redox processes (which depend on the ligands L, L–L, L' and L'–L') is large the first oxidation occurs with retention of geometry; subsequent oxidation at the *cis* site results in isomerisation and the formation of the *trans,trans* trications. Where Δ is small, oxidation of the *trans* site is accompanied by isomerisation at the *cis* centre implying some delocalisation in the mixed-valence dication. The oxidative-isomerisation process therefore provides a probe of the intermetallic interactions in the $Mn_2(\mu\text{-}CN)$ core.

We have recently described[1] chemical and electrochemical studies of the oxidative isomerisation of the complexes *cis*-$[MnX(CO)_2\{P(OPh)_3\}(dppm)]^Z$ **1** [$Z = 0$, X = Br, CN or NCS; $Z = +1$, X = pyridine, NCMe, CNMe or $P(OPh)_3$]. As shown in the 'square scheme'[2] of Fig. 1, the one-electron oxidation of **1** yields $\mathbf{1}^+$ which rapidly isomerises to *trans*-$[MnX(CO)_2\{P(OPh)_3\}(dppm)]^{Z+1}$ $\mathbf{2}^+$.

The redox-induced isomerisation of compound **1** is readily detected by cyclic voltammetry in that an irreversible oxidation wave, due to the sequence $\mathbf{1} \longrightarrow \mathbf{1}^+ \longrightarrow \mathbf{2}^+$, is coupled to a reversible product wave (at a more negative potential) due to the couple $\mathbf{2}^+$–**2**. In addition the *cis* and *trans* geometries are easily distinguished by IR carbonyl spectroscopy, the former giving rise to two bands and the latter resulting in one.

We have therefore studied the cyclic voltammetry and IR carbonyl spectroscopy of complexes $\mathbf{3}^+$–$\mathbf{6}^+$, binuclear analogues of **1** and **2**, and now give details[3] to show how the oxidative-isomerisation process provides insight into the intermetallic interactions within the $Mn(\mu\text{-}CN)Mn$ framework.

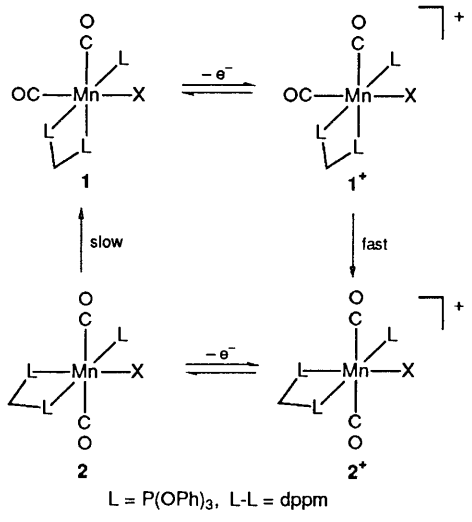

Fig. 1 A 'square scheme' for the oxidative isomerisation of complex **1**

Results and Discussion

Synthetic Studies.—The dimanganese(I) complexes described in this paper (Table 1), having the general formula $[(L–L)L(OC)_2Mn(\mu\text{-}CN)Mn(CO)_2L'(L'–L')][PF_6]$, were generally synthesised by stirring a 1:1 mixture of $[Mn(CN)(CO)_2L(L–L)]$ and $[MnBr(CO)_2L'(L'–L')]$† in CH_2Cl_2 with an excess of $TlPF_6$ in the absence of light [equation (1)]. These reactions were monitored by IR spectroscopy and were usually complete

$$[Mn(CN)(CO)_2L(L–L)] + [MnBr(CO)_2L'(L'–L')] \xrightarrow{TlPF_6} [(L–L)L(OC)_2Mn(\mu\text{-}CN)Mn(CO)_2L'(L'–L')][PF_6] + TlBr \quad (1)$$

within 7 d; filtration followed by the addition of diethyl ether gave the products as orange or yellow precipitates in 40–50% yields. The purification of these precipitates often proved difficult in that the desired binuclear complexes can be contaminated by small quantities of mononuclear impurities or other binuclear isomers with similar solubility. In these cases samples of sufficient purity for elemental analysis and electrochemistry were obtained by fractional crystallisation from CH_2Cl_2–diethyl ether or CH_2Cl_2–hexane. Column

* Throughout this paper, L = L' = $P(OPh)_3$ and L–L = L'–L' = $Ph_2PCH_2PPh_2$ (dppm) unless stated otherwise (in which case any different ligands are specified after the complex number).

† Data for previously unreported mononuclear compounds are given in Table 2.

Table 1 Analytical and IR spectral data[a] for $[PF_6]^-$ salts of complexes 3^+–6^+

					Analysis (%)[b]				$\tilde{\nu}$(CO)[d]/cm^{-1}	
Complex	L	L–L	L′	L′–L′	C	H	N	$\tilde{\nu}$(CN)[c]/cm^{-1}	Mn–C[e]	Mn–N[f]
3^+	$P(OPh)_3$	dppm	$P(OPh)_3$	dppe	*g*			2094	1931s(br)	1931s(br)
3^+	$P(OPh)_3$	dppm	$P(OPh)_3$	dppm	61.1 (61.3)	4.4 (4.2)	0.9 (0.8)	2094	2046w[h], 1933s(br)	2046w[h], 1933s(br)
3^+	$P(OPh)_3$	dppm	$P(OEt)_3$	dppm	*i*			2095	1931	1910m
3^+	$P(OEt)_3$	dppm	$P(OPh)_3$	dppm	*g*			2091	1917	1928
3^+	$P(OPh)_3$	dmpe	$P(OPh)_3$	dmpe	47.3 (47.4)	4.8 (4.6)	1.2 (1.0)[j]	2101	2001w[h], 1914	2001w[h], 1914
4^+	$P(OPh)_3$	dppm	$P(OPh)_3$	dppm	60.5 (60.2)	4.1 (4.1)	0.8 (0.8)[j,k]	2090	1971m, 1921m	2020w[h], 1928
4^+	$P(OPh)_3$	dppm	$P(OEt)_3$	dppm	57.4 (57.9)	4.5 (4.6)	0.9 (0.9)	2098	1970m, 1917	1917
4^+	$P(OEt)_3$	dppm	$P(OPh)_3$	dppm	56.8 (56.8)	4.7 (4.6)	0.9 (0.8)[j]	2097	1960, 1903	2020w[h], 1930
4^+	PEt_3	dppe	$P(OPh)_3$	dppm	59.6 (59.9)	4.8 (4.7)	0.8 (0.9)	2086	1942m, 1885m	2019w[h], 1928
4^+	$P(OPh)_3$	dmpe	$P(OPh)_3$	dmpe	47.6 (47.4)	4.9 (4.6)	1.1 (1.0)[j]	2109	1965m, 1908s	2008w[h], 1908s
5^+	$P(OPh)_3$	dppm	$P(OPh)_3$	dppe	60.5 (60.4)	4.4 (4.2)	1.0 (0.8)[j,k]	2089	1931	1968m, 1900m
5^+	$P(OPh)_3$	dppm	$P(OPh)_3$	dppm	60.8 (61.3)	4.2 (4.2)	0.8 (0.8)	2096	2013w[h], 1931	1968m, 1901m
5^+	$P(OPh)_3$	dppm	$P(OEt)_3$	dppm	57.8 (57.9)	4.7 (4.5)	0.9 (0.9)	2096	2015vw[h], 1931	1955m, 1890m
5^+	$P(OPh)_3$	dppm	PEt_3	dppe	59.9 (59.9)	4.8 (4.7)	0.8 (0.9)	2079	2012vw[h], 1932s(br)	1932s(br), 1871m
6^+	$P(OPh)_3$	dppm	$P(OPh)_3$	dppm	60.1 (60.2)	4.2 (4.1)	0.8 (0.8)[j]	2089	1971s(br), 1917s(br)	1971s(br), 1917s(br)
6^+	$P(OPh)_3$	dppm	$P(OEt)_3$	dppm	56.9 (56.8)	4.6 (4.6)	0.9 (0.8)[j]	2098	1972, 1917	1957, 1891

[a] In CH_2Cl_2. [b] Calculated values in parentheses. [c] Weak. [d] Strong (s) unless otherwise stated; br = broad, m = medium, vw = very weak. [e] Carbonyl stretching frequencies of C-bonded $Mn(CO)_2L(L–L)$ fragment. [f] Carbonyl stretching frequencies for N-bonded $Mn(CO)_2L'(L'–L')$ fragment. [g] Not isolated; IR spectral data from sample generated *in situ* (see text). [h] The symmetry-forbidden A_{1g} (in D_{4h}) stretching vibration. [i] Sample not analysed (see text). [j] Sample analysed as a 0.5 CH_2Cl_2 solvate. [k] Solvent of crystallisation confirmed by ^1H NMR spectroscopy.

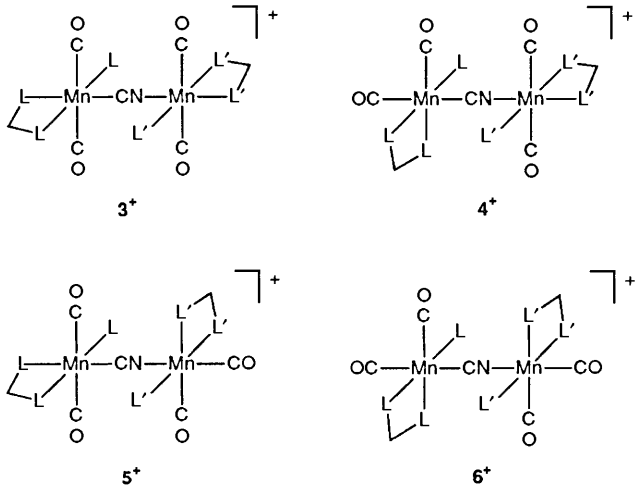

chromatography on alumina–CH_2Cl_2 generally resulted in extensive decomposition although the use of a silica gel–CH_2Cl_2 column was successful with 4^+ [L = PEt_3, L–L = $Ph_2PCH_2CH_2PPh_2$(dppe)].

The binuclear complexes can adopt four isomeric structures, 3^+–6^+, depending on the *cis* or *trans* arrangement of each $Mn(CO)_2$ centre. In addition positional isomerism can occur due to the asymmetry of the cyanide bridge {for example, 4^+ [L = $P(OPh)_3$, L–L = dppm, L′ = $P(OEt)_3$, L′–L′ = dppm] differs from 4^+ [L = $P(OEt)_3$, L–L = dppm, L′ = $P(OPh)_3$, L′–L′ = dppm]}. However, many of the theoretically possible isomers are chemically inaccessible because of the unavailability of suitable mononuclear bromide or cyanide precursors, particularly with the *trans* geometry of **2**. Such *trans* precursors are synthesised by oxidising a neutral *cis* complex to the *trans* cation and then reducing the latter, with retention of configuration, to *trans*-[$MnX(CO)_2L(L–L)$] [*e.g.* X = CN or Br, L = $P(OPh)_3$ or $P(OEt)_3$, L–L = dppm]. The rate of isomerisation of compound **2** to **1** is ligand dependent so that, for example, *trans*-[$MnX(CO)_2(PEt_3)$(dppe)] (X = CN or Br) reverts too rapidly to the *cis* isomer to be isolable.

The complexes listed in Table 1 were characterised by elemental analysis, IR spectroscopy and cyclic voltammetry. The IR carbonyl spectra suggest that there is limited interaction between the two manganese(I) centres in 3^+–6^+ (a suggestion supported by the electrochemical studies described below). Thus, for example, the *trans,cis* complexes show essentially no change in $\tilde{\nu}$(CO) for the C-bonded *trans*-$Mn(CO)_2\{P(OPh)_3\}$-(dppm) fragment as the two carbonyl bands of the N-bound *cis*-$Mn(CO)_2L'(L'–L')$ unit vary with L′ and L′–L′. In addition, the IR data indicate that an N-bound manganese centre is more electron rich than a C-bound analogue (*i.e.* that the former is more readily oxidised than the latter); compare, for example, the carbonyl stretching frequencies of the C-bound *cis* unit of 4^+ [$\tilde{\nu}$(CO) 1971 and 1921 cm^{-1}] with those of the N-bound *cis*-unit of 5^+ [$\tilde{\nu}$(CO) 1968 and 1901 cm^{-1}].

Electrochemistry and Chemical Oxidation of Complexes 3^+–6^+.—Complexes 3^+–6^+ generally undergo two sequential one-electron oxidations, at the potentials given in Table 3. However, the presence of the two manganese(I) redox centres and the occurrence of oxidatively induced isomerisation give rise, in some cases, to complex cyclic voltammetry. In order to interpret the behaviour of the *cis,trans* and *trans,cis* complexes (4^+ and 5^+ respectively) that of the *trans,trans* isomer, 3^+, is described first.

The trans,trans *cations* 3^+. The potential data for three isolated salts of *trans,trans* cations 3^+ are given in Table 3 together with those for four other such species formed as products of the oxidative isomerisation of *cis,trans* and *trans,cis* analogues (see below).

The cyclic voltammograms of 3^+, 3^+ [L′ = $P(OEt)_3$], and 3^+ [L–L = L′–L′ = $Me_2PCH_2CH_2PMe_2$ (dmpe)], the isolated complexes, are straightforward; the two diffusion-controlled ($i_{ox}/v^{\frac{1}{2}}$ = constant) oxidation waves are reversible (i_{red}/i_{ox} = 1.0) (at scan rates, v, between 50 and 500 mV s^{-1}) implying the retention of the *trans,trans* geometry in both the di- and tri-cationic species 3^{2+} and 3^{3+}. Similar behaviour was observed for those *trans,trans* isomers formed *in situ* by oxidative isomerisation.

The potentials of the two oxidation waves show little or no difference on changing dppm for dppe, and a negative shift of only 30 and 80 mV (for the first and second oxidation processes respectively) on replacing dppm by dmpe. However, the substitution of $P(OPh)_3$ by $P(OEt)_3$ or PEt_3 at the N-bonded manganese centre significantly lowers E_1, the potential of the first wave (by 0.13 and 0.22 V respectively) while leaving that of the second wave, E_2, essentially unchanged. Similarly, replacing $P(OPh)_3$ at the C-bonded manganese by $P(OEt)_3$ shifts E_2 to a

Table 2 Analytical, IR spectral,[a] and cyclic voltammetric data[b] for $[MnX(CO)_2L(L\text{–}L)]$

				Analysis[c] (%)					
Geometry	X	L	L–L	C	H	N	ν̃(CN)[d]/cm^{-1}	ν̃(CO)[e]/cm^{-1}	E^f/V
cis	Br	$P(OPh)_3$	dmpe	48.9 (47.9)	4.9 (4.8)	—	—	1957, 1876	0.78(I) (0.24)
cis	Br	$P(OEt)_3$	dppm	52.4 (53.4)	5.2 (5.0)	—	—	1946, 1875	0.72(I) (0.11[g])
cis	Br	PEt_3	dppe		*h*		—	*h*	0.58(I) (0.02[g])
cis	Br	$P(OPh)_3$	dppe		*h*		—	*h*	0.90(I) (0.30[g])
trans	Br	$P(OPh)_3$	dmpe	47.3 (47.9)	4.6 (4.8)	—	—	1997w[i], 1898	0.31(R)
trans	Br	$P(OEt)_3$	dppm	53.8 (53.4)	5.0 (5.0)	—	—	1998w[i], 1905	0.15(R)
cis	CN	$P(OPh)_3$	dmpe	49.4 (49.3)	5.1 (4.9)	2.4 (2.1)[j]	2096	1961, 1896	1.08(I) (0.59[g])
cis	CN	$P(OEt)_3$	dppm	59.2 (59.4)	5.6 (5.4)	2.1 (2.0)	2096	1955, 1896	0.95(I) (0.46[g])
cis	CN	PEt_3	dppe	64.2 (64.3)	6.2 (6.0)	2.3 (2.1)	2090	1936, 1873	0.77(I) (0.32[g])
trans	CN	$P(OPh)_3$	dmpe	53.8 (54.3)	5.2 (5.2)	2.3 (2.3)	2084	2001w[i], 1909	0.62(R)
trans	CN	$P(OEt)_3$	dppm	59.0 (59.4)	5.6 (5.4)	2.1 (2.0)	2079	2001w[i], 1914	0.50(R)

[a] In CH_2Cl_2. [b] In CH_2Cl_2 at a platinum-bead electrode. Under the conditions used the potentials for the couples $[Fe(\eta\text{-}C_5H_5)_2]^+$–$[Fe(\eta\text{-}C_5H_5)_2]$ and $[Fe(\eta\text{-}C_5Me_5)_2]^+$–$[Fe(\eta\text{-}C_5Me_5)_2]$ are 0.47 and −0.09 V respectively. [c] Calculated values in parentheses. [d] Weak. [e] Strong unless otherwise stated. [f] The oxidation peak potential $(E_p)_{ox}$, at a scan rate of 200 mV s^{-1}, is given for an irreversible (I) wave; for a reversible (R) wave the oxidation potential is equal to $[(E_p)_{ox} + (E_p)_{red}]/2$. [g] The reduction peak potential $(E_p)_{red}$, at a scan rate of 200 mV s^{-1}, of the reversible product wave. [h] Data given in ref. 4. [i] The symmetry-forbidden A_{1g} (in D_{4h}) stretching vibration. [j] Sample analysed as a 1.0 CH_2Cl_2 solvate.

Table 3 Cyclic voltammetric data[a] for complexes 3^+–6^+

Complex	L	L–L	L′	L′–L′	E_1[b]/V	E_2[b]/V	ΔE[c]/V
3^+	$P(OPh)_3$	dppm	$P(OPh)_3$	dppe	0.65[d]	1.21	0.56
3^+	$P(OPh)_3$	dppm	$P(OPh)_3$	dppm	0.61	1.22	0.61
3^+	$P(OPh)_3$	dppm	$P(OEt)_3$	dppm	0.46	1.21	0.75
3^+	$P(OEt)_3$	dppm	$P(OPh)_3$	dppm	0.57[e]	1.05	0.48
3^+	$P(OPh)_3$	dppm	PEt_3	dppe	0.38[d]	1.19	0.81
3^+	PEt_3	dppe	$P(OPh)_3$	dppm	0.53[e]	0.98	0.45
3^+	$P(OPh)_3$	dmpe	$P(OPh)_3$	dmpe	0.58	1.14	0.56
4^+	$P(OPh)_3$	dppm	$P(OPh)_3$	dppm	0.66	1.58(I)	0.92
4^+	$P(OPh)_3$	dppm	$P(OEt)_3$	dppm	0.49	1.57(I)	1.08
4^+	$P(OEt)_3$	dppm	$P(OPh)_3$	dppm	0.64	1.40(I)	0.76
4^+	PEt_3	dppe	$P(OPh)_3$	dppm	0.71[f]	1.21(I)	0.50
4^+	$P(OPh)_3$	dmpe	$P(OPh)_3$	dmpe	0.63	1.48(I)	0.85
5^+	$P(OPh)_3$	dppm	$P(OPh)_3$	dppe	0.91	1.50(I)	0.59
5^+	$P(OPh)_3$	dppm	$P(OPh)_3$	dppm	0.89	1.51(I)	0.62
5^+	$P(OPh)_3$	dppm	$P(OEt)_3$	dppm	0.86[f]	—	—
5^+	$P(OPh)_3$	dppm	PEt_3	dppe	0.83(I)	—	—
6^+	$P(OPh)_3$	dppm	$P(OPh)_3$	dppm	1.17(I)	—	—
6^+	$P(OPh)_3$	dppm	$P(OEt)_3$	dppm	1.10(I)	—	—

[a] See footnote *b* in Table 2. [b] Reversible one-electron oxidation unless stated otherwise. Where the process is irreversible (I), the oxidation peak potential $[(E_p)_{ox}]$ at a scan rate of 200 mV s^{-1} is given. [c] $\Delta E = E_2 - E_1$. [d] Data taken from the cyclic voltammogram of the *trans,cis* isomer (see text). [e] Data taken from the cyclic voltammogram of the *cis,trans* isomer (see text). [f] Partially reversible wave, E_1 measured from a cyclic voltammogram taken at a sufficiently high scan rate for the wave to show reversibility.

more negative value while E_1 remains the same. Thus, the systematic variation of L and L′ leads to effective control of ΔE (*i.e.* of $E_2 - E_1$). Such variation results in dramatic changes in the electrochemistry of the *cis,trans* and *trans,cis* isomers, described below.

The dependence of E_1, but not E_2, on L′ (and of E_2, but not E_1, on L) is consistent with the conclusions drawn from the IR carbonyl spectra (see above), namely that the interaction between the two manganese(I) centres is limited and that oxidation occurs at the more electron-rich N-bonded end of the binuclear cation. The additional implication, that localised electron loss gives a trapped-valence dication, is supported by the results of chemical and electrolytic oxidation of 3^+.

The controlled-potential electrolysis (CPE) of cation 3^+ in CH_2Cl_2, at a platinum-basket electrode ($E_{applied}$ 0.8 V, 30 min) resulted in the passage of 0.8 F mol^{-1} and the formation of a dark brown solution. Although the *n* value of 0.8 was rather low, the cyclic and rotating-platinum-electrode voltammograms of the electrolysed solution showed the quantitative formation of 3^{2+}; the wave heights and potentials were virtually identical to those of 3^+ except that the wave centred at 0.61 V corresponded to a reduction process.

The chemical oxidation of cation 3^+ was readily effected by using 1 equivalent of $[NO][PF_6]$ in CH_2Cl_2, the addition of hexane to the filtered brown solution giving a near-quantitative yield of the air-sensitive, purple-black bis(hexafluorophosphate) salt of 3^{2+}. This salt was characterised by elemental analysis (Table 4), and by cyclic voltammetry (CV) and rotating-platinum electrode voltammetry (RPEV) which showed reversible reduction (0.61 V) and oxidation (1.22 V) waves at potentials identical to those of 3^+. Although no other *trans,trans* dications analogous to 3^{2+} have been isolated 3^{2+} [L′ = $P(OEt)_3$] was generated in solution by treating $[NO][PF_6]$ with 3^+ [L′ = $P(OEt)_3$], and three others by similar reactions with the appropriate *cis,trans* or *trans,cis* complexes (see below). Each of these dications shows two carbonyl bands in the IR spectrum* (Table 5). Both are shifted to higher wavenumber than those of the corresponding monocations but one is shifted by only *ca.* 10 cm^{-1} whereas

* In addition to the strong carbonyl bands, the IR spectrum of 3^{2+} shows a cyanide band (2043mw cm^{-1}) lowered in energy when compared with that of 3^+ (2094w cm^{-1}), and a weak absorption at 2065 cm^{-1} which can be assigned to the symmetric stretch of one of the *trans*-dicarbonyl fragments (*i.e.* the A_{1g} vibration in D_{4h} symmetry).

Table 4 Analytical data for bis(hexafluorophosphate) salts of cations 3^{2+} and 4^{2+}

Complex	L′	L′–L′	Yield (%)	Colour	Analysis (%)[a] C	H	N
3^{2+}	$P(OPh)_3$	dppm	87	Purple-black	56.0 (55.8)	4.1 (3.8)	1.0 (0.7)[b]
4^{2+}	$P(OPh)_3$	dppm	85	Grey-blue	56.1 (55.8)	4.1 (3.8)	0.6 (0.7)[b]
4^{2+}	$P(OEt)_3$	dppm	72	Dark blue	52.7 (53.2)	4.1 (4.2)	0.6 (0.7)

[a] Calculated values in parentheses. [b] Analysed as a 0.5 CH_2Cl_2 solvate.

Table 5 IR spectral data[a] for cations 3^{z+}, 4^{2+} and 5^{2+}

Complex	L	L–L	L′	L′–L′	$\tilde{\nu}$(CO)[b]/cm^{-1} $z = 2$	$z = 3$
3^{z+}	$P(OPh)_3$	dppm	$P(OPh)_3$	dppe	1997, 1945m	2005
3^{z+}	$P(OPh)_3$	dppm	$P(OPh)_3$	dppm	2000, 1943m	2009
3^{z+}	$P(OPh)_3$	dppm	$P(OEt)_3$	dppm	1988, 1943m	2007, 2000m(sh)
3^{z+}	$P(OEt)_3$	dppm	$P(OPh)_3$	dppm	1996, 1936m	2009, 2004(sh)
3^{z+}	$P(OPh)_3$	dppm	PEt_3	dppe	1970, 1941m	2005, 1981m
3^{z+}	PEt_3	dppe	$P(OPh)_3$	dppm	—	2005, 1979
4^{2+}	$P(OPh)_3$	dppm	$P(OPh)_3$	dppm	2000ms, 1972, 1934ms	—
4^{2+}	$P(OPh)_3$	dppm	$P(OEt)_3$	dppm	1994, 1973, 1932m	—
4^{2+}	$P(OEt)_3$	dppm	$P(OPh)_3$	dppm	2001, 1963, 1925m	—
5^{2+}	$P(OPh)_3$	dppm	$P(OPh)_3$	dppe	1998, 1966m, 1921m	—
5^{2+}	$P(OPh)_3$	dppm	$P(OPh)_3$	dppm	1997, 1966m, 1921m	—

[a] In CH_2Cl_2. [b] Strong (s) absorptions unless otherwise stated; sh = shoulder.

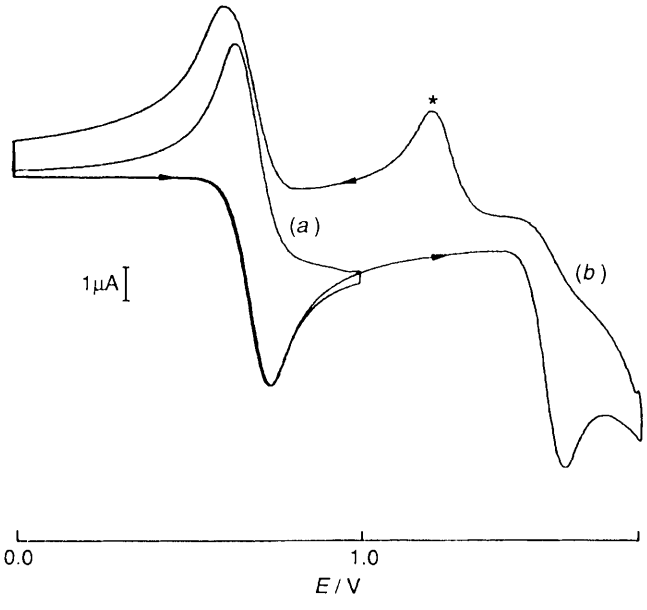

Fig. 2 Cyclic voltammograms of the cation 4^+ (*a*) from 0.0 to 1.0 V and (*b*) from 0.0 to 1.8 V. The reduction peak for the couple 3^{3+}–3^{2+} is labelled with an asterisk.

the second is moved by *ca.* 70 cm^{-1}. The larger shift is similar in magnitude to that observed when *trans*-[Mn(CN)(CO)$_2${P(OPh)$_3$}(dppm)] [$\tilde{\nu}$(CO) 1930 cm^{-1}] is oxidised to its mono-cation [$\tilde{\nu}$(CO) 2002 cm^{-1}], again suggesting that the oxidation of 3^+ is largely confined to one metal centre and that 3^{2+} is trapped-valence dication. Furthermore, the dependence of the energy of the more shifted band on the ligands L′ and L′–L′ clearly shows the N-bonded manganese to be the oxidised centre.

The ESR spectrum of 3^{2+} could only be observed at low temperature [−196 °C, in a CH_2Cl_2–thf (1:2) glass] and poor resolution made the measurement of g and A values impossible. Nevertheless, the spectrum was qualitatively similar to those of the mononuclear low-spin manganese(II) complexes *trans*-[MnX(CO)$_2$L(L–L)]$^+$ [X = Br or CN; L = PEt_3, L–L = dppe; L = $P(OPh)_3$, L–L = dppm][1,5] again suggesting trapped valency for the dication 3^{2+}.

The addition of a second equivalent of [NO][PF_6] to the dications in CH_2Cl_2 led to changes in the IR carbonyl spectra (Table 5) consistent with the formation of the corresponding *trans,trans* trications. Once formed in solution (no trication was isolable) their reactions with the reductant [NBu_4][BH_4] resulted in changes in the IR carbonyl spectra in accord with the stepwise regeneration of the di- and mono-cations.

The overall redox behaviour of the *trans,trans* cations is summarised in Scheme 1. The conclusions drawn, namely that

$$[trans\text{-}Mn^{I}(\mu\text{-}CN)Mn^{I}\text{-}trans]^{+} \underset{+e^-}{\overset{-e^-}{\rightleftharpoons}} [trans\text{-}Mn^{I}(\mu\text{-}CN)Mn^{II}\text{-}trans]^{2+} \underset{+e^-}{\overset{-e^-}{\rightleftharpoons}} [trans\text{-}Mn^{II}(\mu\text{-}CN)Mn^{II}\text{-}trans]^{3+}$$

Scheme 1 Ligands other than the cyanide bridge omitted for clarity

oxidation is stepwise (first at the N-bound manganese) and essentially localised, are now used in the interpretation of the more complex redox reactions of the *cis,trans*, *trans,cis* and *cis,cis* isomers.

The cis,trans *cations* 4^+. The oxidation of the five *cis,trans* cations has been investigated and the associated potentials are given in Table 2. The behaviour of 4^+ (L = PEt_3, L–L = dppe) differs from that of the other four complexes; it is related to that of the *trans,cis* cations and is therefore discussed in the next section.

The cyclic voltammogram of 4^+, shows two waves in the potential range 0.0–1.8 V (Fig. 2). The first wave, when scanned alone [Fig. 2(*a*)] is fully reversible (E° = 0.66 V) and diffusion controlled; the second wave [Fig. 2(*b*)] is chemically irreversible [$(E_p)_{ox}$ = 1.58 V] and accompanied by a product wave [$(E_p)_{red}$ = 1.15 V] which multiple scan CV shows to be reversible and centred at a potential equal to that of the couple 3^{3+}–3^{2+}. Thus, oxidative isomerisation occurs at the *cis*-Mn(CO)$_2$ site *only* when the second oxidation wave is scanned;

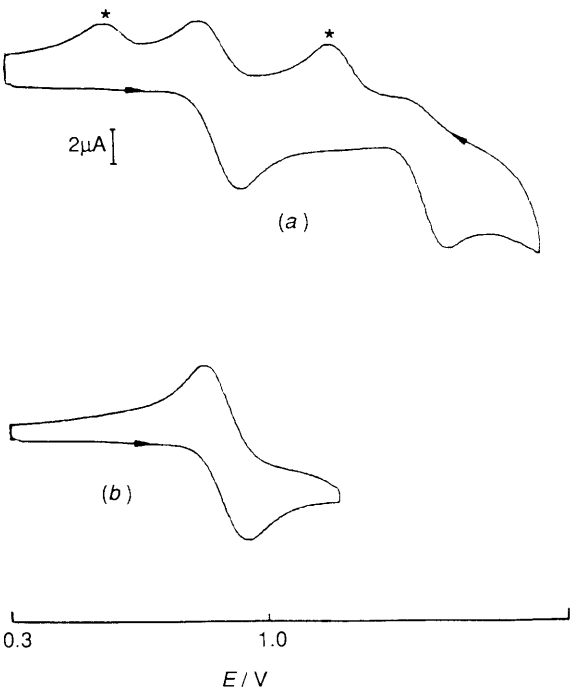

Fig. 3 Cyclic voltammograms of the cation 5^+ (*a*) from 0.3 to 1.8 V and (*b*) from 0.3 to 1.2 V. The reduction peaks of the product couples 3^{3+}–3^{2+} and 3^{2+}–3^+ are labelled with asterisks.

once formed the *cis,trans* trication 4^{3+} undergoes rapid isomerisation to the *trans,trans* trication 3^{3+}. Although the product wave due to the 3^{3+}–3^{2+} couple is clearly evident in Fig. 2(*b*), that due to the couple 3^{2+}–3^+ (which should also be present) is less so. Nevertheless, a comparison of Fig. 2(*a*) and 2(*b*) shows there to be a significant broadening of the reduction peak at *ca.* 0.6 V when the second oxidation wave of 4^+ is scanned. The potentials of the reversible couples 4^{2+}–4^+ (E° = 0.66 V) and 3^{2+}–3^+ (E° = 0.61 V) are insufficiently different to be fully resolved by CV. The cyclic voltammograms of 4^+ [L = $P(OEt)_3$], 4^+ [L′ = $P(OEt)_3$] and 4^+ (L–L = L′–L′ = dmpe) are similar to that of 4^+; the ligand dependence of E_1 (Table 3) is again consistent with loss of the first electron from an N-bonded *trans*-$Mn(CO)_2$ site.

The CPE of cation 4^+ at an applied potential of 0.9 V resulted in the passsage of 0.9 F mol^{-1} (*i.e.* n = 0.9), and a green-brown solution was formed with cyclic and rotating-platinum electrode voltammograms identical to that of the starting material (except for the *reduction* process at 0.66 V). Thus, electrolytic one-electron oxidation of 4^+ leads to the quantitative formation of a dication in which the geometry at both metal sites is retained, *i.e.* the *cis,trans* complex 4^{2+}. Further confirmation of the absence of isomerisation was provided by the IR carbonyl spectrum of the electrolysed solution which showed bands at 2000m, 1972s and 1934ms cm^{-1}. A comparison of this spectrum with that of 4^+ [$\tilde{\nu}$(CO) 1971m, 1928s and 1921m(sh) cm^{-1}] showed an increase in energy of 70 cm^{-1} in the band associated with the N-bound *trans*-$Mn(CO)_2$ unit but very little change in the positions of the two bands of the C-bonded *cis*-$Mn(CO)_2$ group.

Two *cis,trans* dications, 4^{2+} (grey-blue) and 4^{2+} [L′ = $P(OEt)_3$, dark blue], were also synthesised chemically, *via* [NO][PF_6] oxidation of the appropriate monocations. The air-sensitive bis(hexafluorophosphate) salts were characterised by elemental analysis (Table 4), IR carbonyl (Table 5) and ESR spectroscopy, and cyclic voltammetry; their spectroscopic and electrochemical properties fully support the conclusions drawn from similar studies of 3^{2+}, namely that localised oxidation occurs at the N-bonded, *trans*-$Mn(CO)_2$ site.

The oxidation of cation 4^{2+}, again with 1 equivalent of [NO][PF_6], gave CH_2Cl_2 solutions of the *trans,trans* trications 3^{3+}; as expected from the CV study of 4^+, isomerisation does occur once the *cis*-$Mn(CO)_2$ unit is oxidised. As noted above, the addition of [NBu^n_4][BH_4] to 3^{3+} gives 3^+ thus completing a cycle whereby double oxidation followed by double reduction converts 4^+ into the isomeric *trans,trans* cation. This cycle therefore provides an indirect route to the *trans,trans* geometry. It has been used on a preparative scale to give 3^+ from 4^+ but has, as yet, not been exploited further.

The redox chemistry of 4^+, 4^+ [L = $P(OEt)_3$], 4^+ [L′ = $P(OEt)_3$], and 4^+ (L–L = L′–L′ = dmpe) is summarised in Scheme 2.

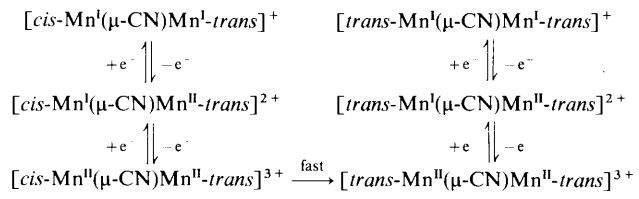

Scheme 2

The trans,cis *cations*, 5^+. The four *trans,cis* cations 5^+, 5^+ (L′–L′ = dppe), 5^+ [L′ = $P(OEt)_3$], and 5^+ (L′ = PEt_3, L′–L′ = dppe) show ligand (L′)-dependent electrochemistry which, taken with the CV study of 4^+ (L = PEt_3, L–L = dppe), provides the first indication that the $Mn_2(\mu\text{-CN})$ dications can exhibit Class II (weakly delocalised) rather than Class I (fully localised) mixed valency (where Classes I and II refer to the Robin–Day classification of mixed-valence complexes[6]).

The cyclic voltammograms of 5^+ and 5^+ (L′–L′ = dppe) are very similar. In the range 0.3–1.8 V the cyclic voltammogram of 5^+ [Fig. 3(*a*)] shows a fully reversible, diffusion-controlled, first oxidation wave at *ca.* 0.9 V [Fig. 3(*b*)] followed by a second, irreversible wave at *ca.* 1.5 V (Table 3); the latter is accompanied by two product waves [$(E_p)_{red}$ = 1.18 and 0.57 V] whose potentials are identical to those for the couples 3^{3+}–3^{2+} and 3^{2+}–3^+.

The potential of the first wave of 5^+ and 5^+ (L′–L′ = dppe), {and of 5^+ [L′ = $P(OEt)_3$] and 5^+ (L′ = PEt_3, L′–L′ = dppe) (see below)} is virtually independent of the nature of L′ and L′–L′ (Table 3), and the reversibility of the wave also suggests that it is associated with oxidation at the C-bonded *trans* site. The potential is *ca.* 200 mV more positive than that for the oxidation of an analogous N-bonded *trans* site (*i.e.* with the same set of ancillary ligands, L′ and L′–L′, in 3^+ or 4^+), a change consistent with the IR carbonyl spectra discussed above which suggested the N-bound end of the Mn(μ-CN)Mn unit to be the more electron rich.

The cyclic voltammograms of cations 5^+ and 5^+ (L′–L′ = dppe) are similar to those of 4^+ (see above) in showing that, *on the time-scale of the experiment*, isomerisation occurs only if the *cis* site is oxidised. However, complexes 5^+ [L′ = $P(OEt)_3$] and 5^+ (L′ = PEt_3, L′–L′ = dppe) show rather different behaviour. On scanning the cyclic voltammogram of 5^+ [L′ = $P(OEt)_3$] from 0.0 to 1.0 V [Fig. 4(*a*)] a partially reversible wave (*e.g.* i_{red}/i_{ox} = 0.8, ν = 200 mV s^{-1}) is observed, accompanied by a reversible product wave with a potential (0.48 V) identical to that for the *trans,trans* couple 3^{2+} [L′ = $P(OEt)_3$]–3^+ [L′ = $P(OEt)_3$]. On scanning the cyclic voltammogram to 1.5 V [Fig. 4(*b*)] the expected irreversible wave due to the oxidation of 5^{2+} [L′ = $P(OEt)_3$] to 5^{3+} [L′ = $P(OEt_3)$] {and isomerisation to 3^{3+} [L′ = $P(OEt)_3$]} is *not* observed. Rather, there is a reversible wave at 1.23 V corresponding to the couple 3^{3+} [L′ = $P(OEt)_3$]–3^{2+} [L′ = $P(OEt)_3$]. Clearly, 5^{2+} [L′ = $P(OEt)_3$] isomerises rapidly to 3^{2+} [L′ = $P(OEt)_3$], *i.e.* isomerisation occurs at the *cis* centre even though only the *trans* site is oxidised.

The cyclic voltammogram of cation 4^+ (L = PEt_3, L–L = dppe) (Fig. 5) is qualitatively similar to that of 5^+ [L′ = $P(OEt)_3$] in that product waves at 0.53 and 0.93 V, assignable

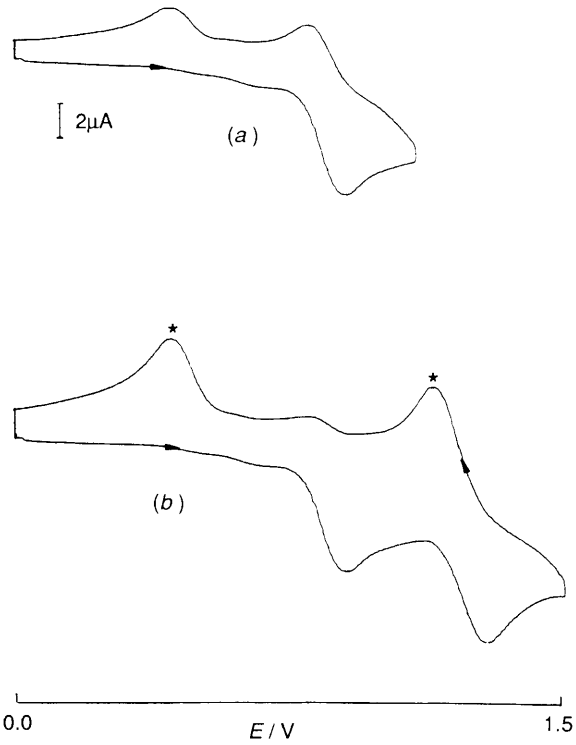

Fig. 4 Cyclic voltammograms of the cation 5^+ [L′ = $P(OEt)_3$] (*a*) from 0.0 to 1.0 V and (*b*) from 0.0 to 1.5 V. The reduction peaks of the product couples 3^{3+}–3^{2+} [L′ = $P(OEt)_3$] and 3^{2+}–3^+ [L′ = $P(OEt)_3$] are labelled with asterisks.

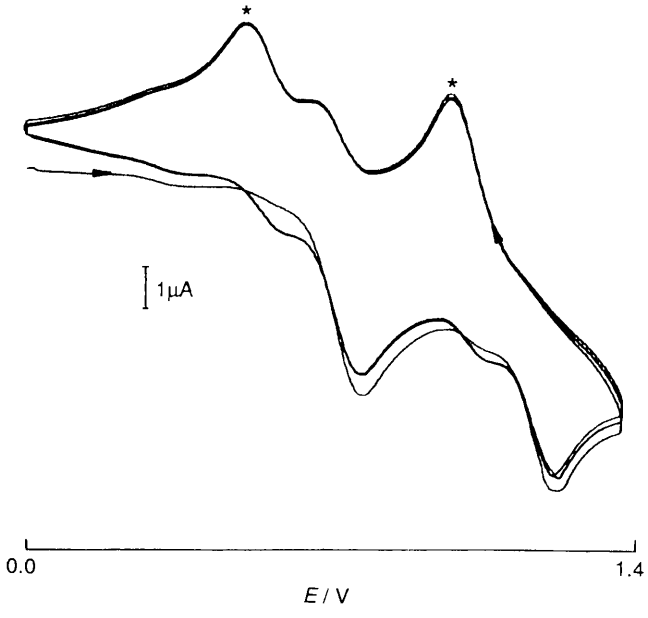

Fig. 5 Multiple scan cyclic voltammogram of the cation 4^+ (L = PEt_3, L–L = dppe) from 0.0 to 1.4 V. The reduction peaks of the product couples 3^{3+}–3^{2+} (L = PEt_3, L–L = dppe) and 3^{2+} 3^+ (L = PEt_3, L–L = dppe) are labelled with asterisks.

to the *trans,trans* dication–cation and trication–dication couples respectively, are observed even if only the first (partially reversible) wave (at 0.71 V) due to the oxidation at the *trans* site is scanned. In this case, however, the isomerisation of 4^{2+} (L = PEt_3, L–L = dppe) to 3^{2+} (L = PEt_3, L–L = dppe) is slow enough for the irreversible oxidation of the former to 4^{3+} (L = PEt_3, L–L = dppe) also to be detected. By contrast, the cyclic voltammogram of 5^+ (L′ = PEt_3, L′–L′ = dppe) from 0.0 to 1.0 V [Fig. 6(*a*)] shows that the rapid isomerisation of 5^{2+} (L′ = PEt_3, L′–L′ = dppe) to 3^{2+} (L′ = PEt_3, L′–L′ = dppe) renders

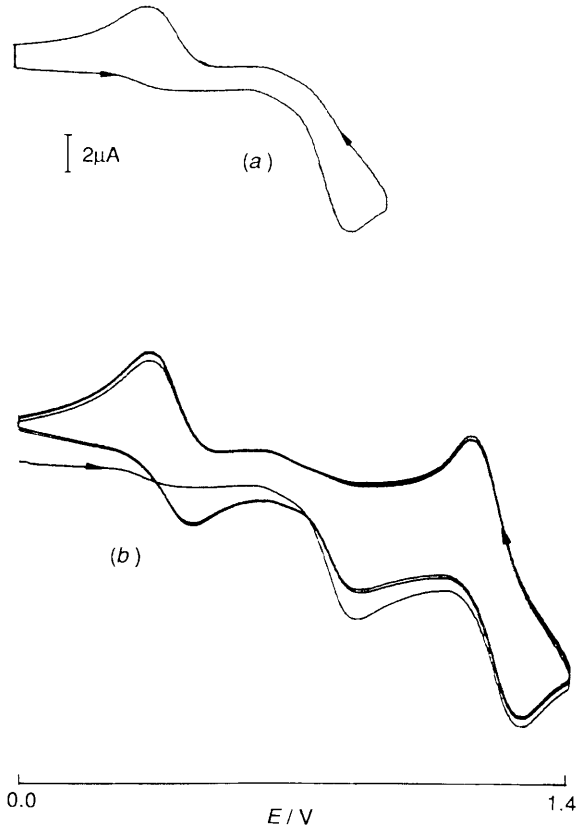

Fig. 6 Cyclic voltammogram of the cation 5^+ (L′ = PEt_3, L′–L′ = dppe), (*a*) single scan from 0.0 to 1.0 V and (*b*) multiple scan from 0.0 to 1.4 V

the first oxidation wave completely irreversible even at 500 mV s^{-1}; the multiple scan cyclic voltammogram from 0.0 to 1.4 V [Fig. 6(*b*)] shows the two product waves at 0.39 and 1.21 V.

Although cation 5^{2+} is stable on the CV time-scale, and therefore differs from 5^{2+} [L′ = $P(OEt)_3$] and 5^{2+} (L′ = PEt_3, L′–L′ = dppe), it cannot be generated chemically or by electrolysis. CPE of 5^+ at 1.1 V (n = 0.9) resulted in a dark brown-purple solution the voltammetry of which (CV and RPEV) showed the quantitative formation of the *trans,trans* dication 3^{2+} [reversible CV waves at 0.61 (reduction) and 1.22 V (oxidation)]. Thus, on the time-scale of electrolysis (*ca.* 20 min) 5^+ behaves in the same way as the other *trans,cis* monocations; oxidation at the C-bound *trans*-manganese(I) site results in isomerisation at the N-bound *cis* centre. The rate of that isomerisation varies with L′ in the order $P(OPh)_3$ < $P(OEt)_3$ < PEt_3.

The electrochemistry of the *trans,cis* cations is summarised in Scheme 3 which is supported by studies of the chemical oxidation of 5^+. A similar scheme applies to 4^+ (L = PEt_3, L–L = dppe).

$$\begin{array}{ccc}
[trans\text{-}Mn^{I}(\mu\text{-}CN)Mn^{I}\text{-}cis]^+ & \xleftarrow{(i)} & [trans\text{-}Mn^{I}(\mu\text{-}CN)Mn^{I}\text{-}trans]^+ \\
+e \uparrow\downarrow -e & & +e \uparrow\downarrow e \\
[trans\text{-}Mn^{II}(\mu\text{-}CN)Mn^{I}\text{-}cis]^{2+} & \xrightarrow{\text{fast}} & [trans\text{-}Mn^{I}(\mu\text{-}CN)Mn^{II}\text{-}trans]^{2+} \\
+e \uparrow\downarrow e & & +e \uparrow\downarrow e \\
[trans\text{-}Mn^{II}(\mu\text{-}CN)Mn^{II}\text{-}cis]^{3+} & \xrightarrow{\text{fast}} & [trans\text{-}Mn^{II}(\mu\text{-}CN)Mn^{II}\text{-}trans]^{3+}
\end{array}$$

Scheme 3 (*i*) slow, L′ = $P(OPh)_3$; fast, L′ = PEt_3

The addition of 1 equivalent of [NO][PF_6] to cation 5^+ in CH_2Cl_2 ultimately (*ca.* 20 min) gave new IR carbonyl bands at 2000 and 1943 cm^{-1} (and a weak cyanide band at 2043 cm^{-1})

due to the formation of $\mathbf{3}^{2+}$ (Table 5). However, an intermediate showing bands at 1997s, 1966m and 1921m cm^{-1} was also observed. These bands may be assigned to the *trans,cis* dication $\mathbf{5}^{2+}$ by comparison with those of $\mathbf{5}^{+}$ [$\tilde{\nu}$(CO) 1968m, 1931s and 1901m cm^{-1}] *i.e.* on oxidation there is a typical shift of 60 cm^{-1} in the band assigned to the *trans*-$Mn(CO)_2$ unit but a relatively small change in the bands associated with the *cis*-$Mn(CO)_2$ group.

The addition of 1 equivalent of $[N(C_6H_4Br\text{-}p)]_3]^+$ to $\mathbf{5}^{+}$, [L′ = $P(OEt)_3$] or $\mathbf{5}^{+}$ (L′ = PEt_3, L′–L′ = dppe) in CH_2Cl_2 rapidly gave the *trans,trans* dications, characterised by their IR carbonyl spectra (Table 5). In these cases the *trans,cis*-dicationic intermediates could not be detected, reflecting the rapidity with which they isomerise (as described above). In all cases a second equivalent of one-electron oxidant gave the *trans,trans* trications.

The reduction of the cation $\mathbf{3}^{3+}$ [L′ = $P(OEt)_3$] with 2 equivalents of $[NBu^n_4][BH_4]$ was carried out on a preparative scale, giving $\mathbf{3}^{+}$ [L′ = $P(OEt)_3$] in good yield. Thus, two-electron oxidation of $\mathbf{5}^{+}$ [L′ = $P(OEt)_3$] followed by two-electron reduction provided an alternative route to the mono-cationic *trans,trans* isomer. By contrast, the reduction of $\mathbf{3}^{3+}$ (L′ = PEt_3, L′–L′ = dppe) [or of $\mathbf{3}^{3+}$ (L = PEt_3, L–L = dppe), generated by double oxidation of $\mathbf{4}^{+}$ (L = PEt_3, L–L = dppe)] gave only the initial *trans,cis* cation $\mathbf{5}^{+}$ (L′ = PEt_3, L′–L′ = dppe) [or $\mathbf{4}^{+}$, (L = PEt_3, L–L = dppe)]. As in the case of the mononuclear complexes the *trans*-$Mn^{I}X(CO)_2(PEt_3)$(dppe) unit isomerises rapidly to the *cis*-manganese(I) form.

The most likely mechanism (Scheme 4) by which the *trans,cis*

$$[\textit{trans}\text{-}Mn^{II}(\mu\text{-}CN)Mn^{I}\textit{-cis}]^{2+} \rightleftharpoons [\textit{trans}\text{-}Mn^{I}(\mu\text{-}CN)Mn^{II}\textit{-cis}]^{2+} \longrightarrow [\textit{trans}\text{-}Mn^{I}(\mu\text{-}CN)Mn^{II}\textit{-trans}]^{2+}$$

Scheme 4

dications $\mathbf{5}^{2+}$ convert into the *trans,trans* isomers [and by which $\mathbf{4}^{2+}$ (L = PEt_3, L–L = dppe) similarly gives $\mathbf{3}^{2+}$ (L = PEt_3, L–L = dppe)] involves intramolecular electron transfer from the *cis*-manganese(I) to the *trans*-manganese(II) site as the first step, a reaction which requires the cyanide bridge to be capable of electron transport.[7] The *cis*-manganese(II) centre then isomerises to the *trans* geometry *via* a non-dissociative twist process as found in mononuclear analogues.[8] Alternative mechanisms involving intermolecular electron transfer cannot be ruled out but they are likely to require complex sequences of steps which intuitively seem less likely.

The stability of the cations $\mathbf{4}^{2+}$ and $\mathbf{4}^{2+}$ [L′ = $P(OEt)_3$] towards isomerisation, and the relative rates of isomerisation of $\mathbf{4}^{2+}$ (L = PEt_3, L–L = dppe) and the *trans,cis* dications to the *trans,trans* analogues (as shown qualitatively by the relative reversibility of the first oxidation waves for the monocations, see above), relate directly to ΔE (the difference between the redox potentials for the first and second oxidation waves, Table 3). Thus, for example, ΔE for those *cis,trans* cations which give stable *cis,trans* dications is *ca.* 1.0 V whereas ΔE for $\mathbf{4}^{+}$ (L = PEt_3, L–L = dppe), $\mathbf{5}^{+}$ and $\mathbf{5}^{+}$ (L′–L′ = dppe) are 0.50. 0.62 and 0.59 V respectively. For the most rapidly isomerised dications $\mathbf{5}^{2+}$ [L′ = $P(OEt)_3$] and $\mathbf{5}^{2+}$ (L = PEt_3, L–L = dppe) ΔE was not measured (the second oxidation waves are not detectable at the moderate scan rates used). It can safely be assumed, however, that $\Delta E < 0.59$ V; as the donor ability of L′ is increased, E_2 will become more negative (*cf.* the potential data for the *trans,trans* complexes in Table 3).

The rates and mechanisms of these redox-induced isomerisations require additional study. Nevertheless, it is clear that the redox reactions of the mixed-valence dications, whether inter- or intra-molecular, can be systematically altered by changing the ligands L, L′, L–L and L′–L′.

The cis,cis *cations*, $\mathbf{6}^{+}$. For the sake of completeness, two complexes with the *cis,cis* geometry have been studied. As might be expected from the behaviour of the related *cis,trans* and *trans,cis* cations, the cyclic voltammetry of the *cis,cis* isomers was complex; isomerisation can occur at either or both *cis* sites. In addition the first oxidation process observed occurs at a rather positive potential (Table 3).

The cyclic voltammograms of cations $\mathbf{6}^{+}$ and $\mathbf{6}^{+}$ [L′ = $P(OEt)_3$] were poorly defined but show two irreversible oxidation waves in the potential range 0.0–1.8 V. The potential of the first wave is dependent on the ligand L′ (Table 3) but that of the second is less so (1.58 and 1.61 V respectively). Note, however, that because isomerisation undoubtedly occurs at the first oxidation step, the second wave is not due to the oxidation of $\mathbf{6}^{2+}$ to $\mathbf{6}^{3+}$. If oxidation occurs at the N-bonded site, as expected from the dependence of E_1 on L′ and from the studies of the other isomers reported above, then the second wave is most likely due to the oxidation of $\mathbf{4}^{2+}$ {and $\mathbf{4}^{2+}$ [L′ = $P(OEt)_3$]} (at 1.58 and 1.57 V respectively, Table 2) to the corresponding trications (which then, of course, isomerise to the *trans,trans* isomers). This interpretation is borne out by the chemical oxidation of $\mathbf{6}^{+}$ [L′ = $P(OEt)_3$]. On adding 1 equivalent of $[NO][PF_6]$ to $\mathbf{6}^{+}$ [L′ = $P(OEt)_3$] in the electrochemical cell a dark blue solution was generated having an identical cyclic voltammogram to that of $\mathbf{4}^{+}$ [L′ = $P(OEt)_3$] but with a rotating-platinum electrode voltammogram and IR spectrum [ν(CO) 1994s, 1973s and 1932m cm^{-1}] showing the presence of the dication $\mathbf{4}^{2+}$ [L′ = $P(OEt)_3$]. As deduced above, oxidative isomerisation at the N-bonded site of $\mathbf{6}^{+}$ [L′ = $P(OEt)_3$] has clearly occurred. A second equivalent of $[NO][PF_6]$ gave the *trans,trans* trication $\mathbf{3}^{3+}$ [L′ = $P(OEt)_3$]; the electrochemistry of the *cis,cis* complexes $\mathbf{6}^{+}$ and $\mathbf{6}^{+}$ [L′ = $P(OEt)_3$] can therefore be summarised by Scheme 5.

$$\begin{array}{ccc} [\textit{cis}\text{-}Mn^{I}(\mu\text{-}CN)Mn^{I}\textit{-cis}]^{+} & & [\textit{trans}\text{-}Mn^{I}(\mu\text{-}CN)Mn^{I}\textit{-trans}]^{+} \\ \quad +e \uparrow\downarrow e & & \quad +e \uparrow\downarrow e \\ [\textit{cis}\text{-}Mn^{I}(\mu\text{-}CN)Mn^{II}\textit{-cis}]^{2+} & & [\textit{trans}\text{-}Mn^{I}(\mu\text{-}CN)Mn^{II}\textit{-trans}]^{2+} \\ \quad \downarrow \text{fast} & & \quad +e \uparrow\downarrow -e \\ [\textit{cis}\text{-}Mn^{I}(\mu\text{-}CN)Mn^{II}\textit{-trans}]^{2+} & \xrightarrow{-e^-} & [\textit{trans}\text{-}Mn^{II}(\mu\text{-}CN)Mn^{II}\textit{-trans}]^{3+} \end{array}$$

Scheme 5

Conclusion

The oxidative isomerisation process observed for mononuclear species such as **1** and **2** has allowed a semiquantitative study of the interactions between the two metal sites in the cyanide-bridged dimanganese isomers $\mathbf{3}^{+}$–$\mathbf{6}^{+}$.

Each binuclear complex studied shows two oxidation waves in their cyclic voltammogram. Where the potentials of those waves are substantially different, both IR carbonyl spectroscopy and CV suggest localised, stepwise oxidation of the two metal sites (*trans* sites are more readily oxidised than analogous *cis* sites, and an N-bonded site is more readily oxidised than a C-bonded analogue). The IR and ESR spectra of three isolated dications (and others generated in solution) support localised electronic structures. As the redox potentials of the two waves become more similar, intermetallic interaction, *via* the cyanide bridge, increases. Thus, isomerisation at a *cis* site can be induced by *trans* site oxidation.

The electronic structure of the mixed-valence dications remains to be studied in detail in order to quantify the extent of intermetallic interaction. For example, a striking feature of the dications is their colour (Table 4) which indicates Class II (weak interaction) rather than Class I (no interaction) behaviour. The latter class of complex might be expected to be similar in colour to the mononuclear manganese(I) [**1** or **2** (yellow to orange)] or manganese(II) ($\mathbf{2}^{+}$, red to purple) complexes. Further spectroscopic studies are in progress.

Experimental

The preparation, purification, and reactions of the complexes

described were carried out under an atmosphere of dry nitrogen, using dried, distilled, deoxygenated solvents. Unless stated otherwise, the complexes are air-stable solids, dissolving in polar solvents such as CH_2Cl_2 to give moderately air-sensitive solutions. All the reactions were carried out in flasks shielded from light by aluminium foil.

The compounds *cis*- and *trans*-[$MnBr(CO)_2${$P(OPh)_3$}(dppm)], *cis*-[$MnBr(CO)_2L$(dppe)] [L = $P(OPh)_3$ or PEt_3],[4] and *cis*- and *trans*-[$Mn(CN)(CO)_2${$P(OPh)_3$}(dppm)][9] were prepared by published methods or modification thereof. The salts [NO][PF_6], $TlPF_6$ and AgCN were purchased from Fluorochem, Strem Chemicals and BDH respectively.

Infrared spectra were recorded on Nicolet MX-5 FT or ZDX spectrometers, or a Perkin-Elmer PE-257 spectrometer with calibration against the absorption band of polystyrene at 1601 cm^{-1}. X-Band ESR spectra were recorded on a Varian Associates 4502/15 instrument and were calibrated against a solid sample of the diphenylpicrylhydrazyl (dpph) radical.

Electrochemical studies were carried out using an Amel Electrochemolab, or an EG and G model 273 potentiostat, in conjunction with a three-electrode cell. For cyclic voltammetry the auxiliary electrode was a platinum wire and the working electrode was a platinum bead. The reference was an aqueous saturated calomel electrode (SCE) separated from the test solution by a fine-porosity frit and an agar bridge saturated with KCl. A similar configuration was used for controlled-potential electrolysis but with a platinum-gauze basket as the working electrode and a platinum spiral as the auxiliary electrode. Voltammetry used a platinum-bead electrode rotated at 600 revolutions min^{-1}. Solutions were 0.5×10^{-3} or 1.0×10^{-3} mol dm^{-3} in complex and 0.1 mol dm^{-3} in [NBu_4][PF_6] as the supporting electrolyte. Under these conditions, E^0 for the couples $[Fe(\eta\text{-}C_5H_5)_2]^+$–$[Fe(\eta\text{-}C_5H_5)_2]$ and $[Fe(\eta\text{-}C_5Me_5)_2]^+$–$[Fe(\eta\text{-}C_5Me_5)_2]$ are 0.47 and −0.09 V respectively.

Microanalyses were carried out by the staff of the Microanalytical Services of the School of Chemistry, University of Bristol, and of the University of Oviedo.

cis-[1,2-*Bis*(*diphenylphosphino*)*ethane*]*bromodicarbonyl*(*triethylphosphine*)*manganese*, *cis*-[$MnBr(CO)_2(PEt_3)$(dppe)].—A mixture of *fac*-[$MnBr(CO)_3$(dppe)] (5.7 g, 9.3 mmol) and PEt_3 (4.1 g, 35 mmol) in toluene (100 cm^3) was heated under reflux for 2.5 h. The orange solution was evaporated to dryness to give an orange oil which was redissolved in CH_2Cl_2 (5 cm^3) and chromatographed on an alumina–hexane column (25 × 2.5 cm). Elution with CH_2Cl_2–hexane (1:1) gave an orange solution. Removal of the solvent gave the product as a yellow solid, yield 5.3 g (81%).

The complex *cis*-[$MnBr(CO)_2${$P(OEt)_3$}(dppm)] was prepared similarly from *fac*-[$MnBr(CO)_3$(dppm)] and $P(OEt)_3$ (1:1.2 mol equivalents). The reaction was complete after 1 h and elution of the product from an alumina–hexane column required CH_2Cl_2–hexane (2:3). Further purification by dissolution in Et_2O–hexane (1:2), and cooling to −78 °C to induce precipitation, gave the product as a yellow solid, yield 45%.

The complex *cis*-[$MnBr(CO)_2${$P(OPh)_3$}(dmpe)] was prepared by the method in ref. 4.

cis-[1,2-*Bis*(*diphenylphosphino*)*ethane*]*dicarbonylcyano*(*triethylphosphine*) *manganese*, *cis*-[$Mn(CN)(CO)_2(PEt_3)$(dppe)].—A mixture of *cis*-[$MnBr(CO)_2(PEt_3)$(dppe)] (1.38 g, 1.95 mmol) and AgCN (0.35 g, 2.60 mmol) in CH_2Cl_2 (50 cm^3) was stirred for 16 h and then filtered through Celite. To the filtrate was added a solution of $Na_2S_2O_3$ (2 g) in water (10 cm^3) and the mixture vigorously stirred for 1 h. The CH_2Cl_2 layer was dried with anhydrous $MgSO_4$, filtered, and reduced in volume before hexane (40 cm^3) was added to give a yellow precipitate. The product was purified by dissolution in CH_2Cl_2, filtration, addition of hexane, and partial removal of the solvent to induce precipitation. Washing with hexane (2 × 20 cm^3) gave yellow microcrystals, yield 0.7 g (55%).

The complexes *cis*-[$Mn(CN)(CO)_2L$(L–L)] [L = $P(OEt)_3$, L–L = dppm; L = $P(OPh)_3$, L–L = dmpe] were prepared similarly.

trans-[*Bis*(*diphenylphosphino*) *methane*]*bromodicarbonyl*(*triethyl phosphite*)*manganese*, *trans*-[$MnBr(CO)_2${$P(OEt)_3$}(dppm)].—To a solution of *cis*-[$MnBr(CO)_2${$P(OEt)_3$}(dppm)] (81 mg, 0.11 mmol) in CH_2Cl_2 (10 cm^3) was added [NO][PF_6] (21 mg, 0.12 mmol) and the mixture stirred for 15 min before being filtered through Celite. To the filtrate was added hydrazine monohydrate (0.2 cm^3) with stirring for 15 min. The CH_2Cl_2 layer was dried with anhydrous $MgSO_4$ for 30 min, filtered through Celite, and reduced in volume before the addition of hexane (20 cm^3). The solution was cooled to −78 °C to give a red precipitate which was washed with cold hexane and dried *in vacuo*, yield 56 mg (70%).

The complex *trans*-[$MnBr(CO)_2${$P(OPh)_3$}(dmpe)] was prepared similarly.

trans-[*Bis*(*diphenylphosphino*)*methane*]*dicarbonylcyano*(*triethyl phosphite*)*manganese*, *trans*-[$Mn(CN)(CO)_2${$P(OEt)_3$}(dppm)].—A deep blue solution of [$N(C_6H_4Br\text{-}p)_3$][PF_6] {prepared by stirring $N(C_6H_4Br\text{-}p)_3$ (0.31 g, 0.65 mmol) in CH_2Cl_2 (30 cm^3) with [NO][PF_6] (0.13 g, 0.74 mmol) for 15 min (while passing a rapid stream of nitrogen gas through the mixture)} was filtered into *cis*-[$Mn(CN)(CO)_2${$P(OEt)_3$}(dppm)] (0.44 g, 0.65 mmol) in CH_2Cl_2 (30 cm^3). After 20 min the red-purple solution, containing *trans*-[$Mn(CN)(CO)_2${$P(OEt)_3$}(dppm)]$^+$, was filtered and then added dropwise, over 30 min, to a rapidly stirred mixture of $N_2H_4{\cdot}H_2O$ (0.4 cm^3) in CH_2Cl_2 (100 cm^3). The resulting yellow mixture was then filtered through Celite, washed with water (20 cm^3), and then reduced in volume to *ca.* 10 cm^3 *in vacuo*. Addition of hexane (80 cm^3) gave a yellow powder which was purified by dissolution in CH_2Cl_2, filtration, and precipitation with hexane–diethyl ether, yield 0.32 g (70%).

The complex *trans*-[$Mn(CN)(CO)_2${$P(OPh)_3$}(dmpe)] was prepared similarly.

Synthesis of trans,trans-[(L–L)$L(OC)_2Mn(\mu\text{-}CN)Mn(CO)_2$-L′(L′–L′)][$PF_6$] $\mathbf{3}^+$.—A mixture of *trans*-[$MnBr(CO)_2$-{$P(OPh)_3$}(dppm)] (0.32 g, 0.36 mmol), *trans*-[$Mn(CN)(CO)_2$-{$P(OPh)_3$}(dppm)] (0.30 g, 0.36 mmol) and $TlPF_6$ (0.17 g, 0.49 mmol) in CH_2Cl_2 (25 cm^3) was stirred until the reaction was adjudged complete by IR spectroscopy (*ca.* 7 d). The mixture was filtered and concentrated *in vacuo* (*ca.* 5 cm^3). Slow addition of diethyl ether gave an orange solid, $\mathbf{3}^+$, which was purified by dissolution in CH_2Cl_2, filtration, and addition of diethyl ether to induce precipitation, yield 0.28 g (44%).

The *trans,trans* complex $\mathbf{3}^+$ (L–L = L′–L′ = dmpe), the *cis,trans* complexes $\mathbf{4}^+$, $\mathbf{4}^+$ [L = $P(OEt)_3$], $\mathbf{4}^+$ [L′ = $P(OEt)_3$], $\mathbf{4}^+$ (L = PEt_3, L–L = dppe) and $\mathbf{4}^+$ (L–L = L′–L′ = dmpe), the *trans,cis* complexes $\mathbf{5}^+$, $\mathbf{5}^+$ (L′–L′ = dppe), $\mathbf{5}^+$ [L′ = $P(OEt)_3$] and $\mathbf{5}^+$ (L′ = PEt_3, L′–L′ = dppe), and the *cis,cis* complexes $\mathbf{6}^+$ and $\mathbf{6}^+$ [L′ = $P(OEt)_3$] were prepared similarly, from the appropriate [$Mn(CN)(CO)_2L$(L–L)] and [$MnBr(CO)_2L'$(L′–L′)] precursors.

Synthesis of $\mathbf{3}^+$ [L′ = $P(OEt)_3$] *from* $\mathbf{5}^+$ [L′ = $P(OEt)_3$].—To a solution of the cation $\mathbf{5}^+$ [L′ = $P(OEt)_3$] (40 mg, 24 μmol) in CH_2Cl_2 (10 cm^3) was added [NO][PF_6] (13 mg, 74 μmol). After stirring for 20 min the black solution was filtered and then treated with [NBu_4][BH_4] (15 mg, 59 μmol). The resulting orange solution was filtered and hexane (20 cm^3) added. Partial evaporation of the solvent *in vacuo* gave the product as orange microcrystals, crude yield 32 mg (80%). The product was contaminated with [NBu_4][PF_6] but was sufficiently pure to give good cyclic voltammetric data.

The complexes $\mathbf{4}^+$ and $\mathbf{4}^+$ [L′ = $P(OEt)_3$] were similarly

synthesised from the corresponding *cis,cis* isomer on reaction with $[NO][PF_6]$ (1:1 ratio) followed by treatment with 1 equivalent of $[NBu_4][BH_4]$.

Synthesis of trans,trans-$[(dppm)\{(PhO)_3P\}(OC)_2Mn(\mu\text{-}CN)Mn(CO)_2\{P(OPh)_3\}(dppm)][PF_6]_2$ $\mathbf{3}^{2+}$.—To a stirred solution of the cation $\mathbf{3}^+$ (0.16 g, 0.09 mmol) in CH_2Cl_2 (20 cm^3) was added $[NO][PF_6]$ (16 mg, 0.09 mmol). After 20 min the dark brown solution was filtered and concentrated *in vacuo* to *ca.* 3 cm^3. Addition of hexane (40 cm^3) gave an oily purple-black solid which was washed with diethyl ether (20 cm^3) and then purified by dissolution in CH_2Cl_2, filtration, addition of hexane and partial removal of the solvent to induce precipitation, yield 0.15 g (87%). The purple-black microcrystalline solid is air-sensitive but may be stored at −20 °C under nitrogen. It is soluble in polar solvents such as CH_2Cl_2, thf, or acetone to give black-purple solutions which rapidly decompose in air.

The *cis,trans* dication $\mathbf{4}^{2+}$ was prepared similarly from $\mathbf{4}^+$.

Synthesis of cis,trans-$[(dppm)\{(PhO)_3P\}(OC)_2Mn(\mu\text{-}CN)Mn(CO)_2\{P(OEt)_3\}(dppm)][PF_6]_2$ $\mathbf{4}^{2+}$ [L′ = $P(OEt)_3$].—To a stirred solution of the cation $\mathbf{6}^+$ [L′ = $P(OEt)_3$] (0.19 g, 0.12 mmol) in CH_2Cl_2 (20 cm^3) was added $[NO][PF_6]$ (23 mg, 0.13 mmol). After 20 min the dark blue solution was filtered and concentrated *in vacuo* to *ca.* 5 cm^3. Addition of hexane (30 cm^3) gave an oily blue solid which was washed with toluene (2 × 20 cm^3) and then purified from CH_2Cl_2–hexane, as above, to give a dark blue microcrystalline solid, yield 0.15 g (72%). The solid complex has similar physical properties to the *trans,trans* dication $\mathbf{3}^{2+}$ described above.

Acknowledgements

We thank the SERC for a research studentship (to I. C. Q.) and a postdoctoral research assistantship (to G. H. W.), and the Spanish Direccion General de Investigación Cientifica y Técnica for support.

References

1 N. G. Connelly, K. A. Hassard, B. J. Dunne, A. G. Orpen, S. J. Raven, G. A. Carriedo and V. Riera, *J. Chem. Soc., Dalton Trans.*, 1988, 1623.
2 A. Vallat, M. Person, L. Roullier and E. Laviron, *Inorg. Chem.*, 1987, **26**, 332; A. M. Bond, S. W. Carr and R. Colton, *Organometallics*, 1984, **3**, 541 and refs. therein.
3 G. A. Carriedo, N. G. Connelly, M. C. Crespo, I. C. Quarmby and V. Riera, *J. Chem. Soc., Chem. Commun.*, 1987, 1806.
4 F. Bombin, G. A. Carriedo, J. A. Miguel and V. Riera, *J. Chem. Soc., Dalton Trans.*, 1981, 2049.
5 A. L. Rieger, P. H. Rieger and N. G. Connelly, unpublished work.
6 M. B. Robin and P. Day, *Adv. Inorg. Chem. Radiochem.*, 1967, **10**, 247.
7 See, for example, C. A. Bignozzi, M. T. Indelli and F. Scandola, *J. Am. Chem. Soc.*, 1989, **111**, 5192; L. P. Michiels, G. Kolks, E. R. Nesbitt, P. T. Dimauro, R. M. Kirchner and J. V. Waszczak, *Inorg. Chim. Acta*, 1985, **100**, 211; R. E. Hester and E. M. Nour, *J. Chem. Soc., Dalton Trans.*, 1981, 939.
8 A. M. Bond, B. S. Grabaric and Z. Grabaric, *Inorg. Chem.*, 1978, **17**, 1013.
9 G. A. Carriedo, M. C. Crespo, V. Riera, M. G. Sanchez, M. L. Valin, D. Moreiras and X. Solans, *J. Organomet. Chem.*, 1986, **302**, 47.

Received 30*th July* 1990; *Paper* 0/03469J